Applied Catalysis A, General 605 (2020) 117798

Contents lists available at ScienceDirect

Applied Catalysis A, General

journal homepage: www.elsevier.com/locate/apcata

Gallium and tin exchanged Y zeolites for glucose isomerisation and 5-hydroxymethyl furfural production

Ryan Oozeerally[a], John Pillier[a], Emre Kilic[a], Paul B.J. Thompson[b,c], Marc Walker[d], Benjamin E. Griffith[d], John V. Hanna[d], Volkan Degirmenci[a,*]

[a] School of Engineering, University of Warwick, CV4 7AL, Coventry, UK
[b] Department of Physics, Liverpool, L69 3BX, UK
[c] XMaS UK CRG Beam Line, European Synchrotron Radiation Facility, 38000 Grenoble, France
[d] Department of Physics, University of Warwick, CV4 7AL, Coventry, UK

ARTICLE INFO

Keywords:
HMF
Glucose
Isomerisation
Biomass
Zeolite

ABSTRACT

This study demonstrates the use of gallium and tin modified Y zeolites as catalysts for the conversion of glucose into fructose, mannose and 5-Hydroxymethyl furfural. These catalysts can be synthesised via a simple and scalable procedure that uses commercially available Y zeolite. The catalysts were characterised by various techniques including elemental analysis, electron microscopy, nitrogen physisorption, X-ray diffraction, X-ray photoelectron spectroscopy, ultraviolet-visible spectroscopy, solid state nuclear magnetic resonance spectroscopy and X-ray absorption near edge spectroscopy. It is found that tin containing Y zeolite generate a glucose conversion of 36 % and total product yield of 17 % in water. Meanwhile, gallium containing Y zeolite shows an HMF yield of 33 % when reactions were conducted in DMSO. The recyclability of tin and gallium containing Y zeolites were studied in DMSO and the activities of both materials were shown to remain stable. Furthermore, the spent catalysts can be regenerated via calcination in air.

1. Introduction

Biomass derived platform molecules, such as 5-hydroxylmethyl furfural (HMF), could play a key role in reducing the global dependence on fossil fuel resources. [1,2] HMF has the potential to enable the production of bulk chemicals for polymer, fine chemical and pharmaceutical industries and therefore could pave the wave for a future biorefinery [3,4]. In literature it has been shown that HMF can be easily produced via the dehydration of fructose. [5,6] However, the conversion of glucose, the main constituent of cellulosic biomass, remains challenging. A scalable and industrially applicable heterogeneous catalytic system is highly sought [7,8]. A process utilising the glucose will enable the use of vast cellulosic biomass resources and thus it could accelerate the transition from petroleum to biomass-based chemical industry in a cost effective way [9].

Tin containing beta zeolite (Sn-beta) has attracted great attention over the last decade due to its high selectivity for glucose isomerisation into fructose. [10] Despite its high selectivity, Sn-beta has some drawbacks. First, the traditional synthesis of Sn-beta requires long synthesis times and highly toxic hydrofluoric acid which makes its industrial application challenging. Secondly, Sn-beta suffers from the rapid deactivation under hydrothermal reaction conditions [11] and it has been shown that the use of Sn-beta in a fixed bed reactor leads to the irreversible destruction of the catalyst [12]. Isomerisation of glucose into fructose over Sn-beta needs to be coupled with the consecutive dehydration of fructose into HMF. Preferably, a single step conversion from glucose to HMF could be more cost efficient. The co-use of mineral acids in a one pot reaction have been reported [13], however this further reduces catalyst stability in strongly acidic conditions.

Sn-beta [14–16] and Sn-MFI [17–19] zeolites as well as Sn containing mesoporous silicas [20–22] and acidic resins [23] were extensively studied and reported in literature [24–26]. However, the potential of other zeolite topologies has not been fully explored to date. Considering the vast range of known zeolite types, this remains to be a relatively less studied area. In this respect, zeolite Y is a promising catalyst because it is one of the most widely used catalysts in petrochemical industry [27]. With regards to glucose diffusivity, zeolite Y has an advantage of possessing large pore network, where glucose molecules were shown to diffuse into. [28] Moreover, zeolite Y has been reported to be a promising support for the base catalysed conversion of glucose when its sodium form is doped with magnesium oxide [29–31]. Meanwhile, leaching of the metal species was observed

* Corresponding author.
E-mail address: v.degirmenci@warwick.ac.uk (V. Degirmenci).

https://doi.org/10.1016/j.apcata.2020.117798
Received 15 June 2020; Received in revised form 31 July 2020; Accepted 19 August 2020
Available online 22 August 2020
0926-860X/ © 2020 The Author(s). Published by Elsevier B.V. This is an open access article under the CC BY license (http://creativecommons.org/licenses/by/4.0/).

similar to other reports on cation-exchanged A, X, and, Y zeolites [32]. Among various Mg-promoted zeolite structures, only zeolite Y was observed to recover its initial activity after reactivation in air [31].

Glucose conversion over solid-acid zeolites including zeolite Y, mordenite, ZSM-5 and beta were reported in ionic liquid media with promising conversions and selectivity. [33] However, the use of ionic liquid limits its application because of its high cost, toxicity and potential difficulties in product separation. To design a scalable green process, water is the preferred solvent. Iron doped zeolite Y [34,35], MFI [36], and montmorillonites [37] were reported to be active in glucose conversion. However, regardless of the topology, these solid-acid zeolites were poorly selective towards HMF, yielding levulinic and formic acids as the main products especially under low pH and long reaction times.

In this work, we explored the effect of Sn and Ga addition in zeolite Y on the performance for glucose conversion at relatively low temperature (140 °C) in water, 0.1 M HCl, and DMSO. More recently, it has been shown that the incorporation of Sn [38,39] and Ga [40,41] in Zeolite Y results in stable catalysts in organic solvents for the production of various biomass based green chemicals, such as C_1–C_4 alkyl lactates. Unlike beta zeolite, the structure of zeolite Y contains sodalite cavities and super cage structures. [27,42] Conventional zeolite Y has weak acidity and it is typically hydrothermally unstable with its high aluminium (Al) content (Si/Al < 3.0). [43]. For industrial application, the conventional zeolite Y is replaced by high silica ultra-stable Y zeolite (USY) by removing Al from its framework. [44] The aluminium may reside outside the zeolite Y crystals and the presence of extra framework aluminium leads to improved hydrothermal stability, increased Lewis acidity, and enhanced catalytic activity for reactions that require strong Brønsted acid sites, which are desirable criteria for glucose conversion into HMF. While utilising a simple and scalable catalyst synthesis method, we demonstrate the application of Sn and Ga containing zeolite Y in the isomerization of glucose and production of HMF in water, 0.1 M HCl and DMSO. The recyclability of Sn and Ga materials are also explored in these solvents. Finally, in-situ XANES analysis is employed to better understand the behaviour of Sn and Ga active sites during reactions.

2. Experimental

2.1. Synthesis of catalysts

Zeolite Y catalyst was obtained from Alfa Aesar (#45870, SiO_2/Al_2O_3 mole ratio 30:1, proton form, HY, CAS: 1318−02-1). Dealumination of zeolite Y was performed based on methods adopted from literature [39]. First 5 g of HY was placed in a round bottom flask and 50 mL of 8 M nitric acid solution was added. Second, the mixture was stirred in at 80 °C for 20 h under reflux. After cooling to room temperature, the catalyst was recovered via filtration and washed with deionized water. Finally, the resulting solid was dried at 80 °C and denoted as deAl-HY. For the preparation of Tin (Sn) and Gallium (Ga) containing zeolite Y an adapted incipient wetness technique was applied. Typically, a metal containing precursor solution was made by dissolving 0.118 g of Tin (IV) Chloride Pentahydrate (99.9 % VWR) or 0.147 g of Gallium (III) Nitrate Hydrate (99.9 % Fisher Scientific) in 0.739 mL of demi water. Then, the metal precursor solution was added dropwise on 1 g of deAl-HY. The resulting mixtures were stirred before drying at 80 °C for 24 h. Finally, the samples were calcined at 550 °C (at a heating rate of 1 °C min^{-1}) for 5 h. The Sn and Ga modified zeolites were denoted as Sn-deAl-HY and Ga-deAl-HY respectively.

2.2. Characterization of catalysts

Powder X-ray Diffraction (XRD) patterns were recorded on a Panalytical X'Pert Pro spectrometer equipped with a monochromatic Cu $K_{\alpha 1}$ radiation and a PIXcel solid-state detector, in the 2θ range of 5–40 ° with a scanning speed of 0.05° min^{-1}.

Nitrogen sorption isotherms were measured at −196 °C on a Micromeritics ASAP2020 instrument in static measurement mode. The samples were outgassed at 450 °C for 8 h prior to the sorption measurements. The Brunauer-Emmett-Teller (BET) equation was used to calculate the specific surface area (S_{BET}) from the adsorption branch obtained between p/p_0 0.05 and 0.25. The total pore volume (V_{tot}) is calculated at $p/p_0 = 0.97$. The mesopore volume (V_{meso}) and mesopore size distribution were calculated using the Barrett-Joyner-Halenda (BJH) method on the adsorption branch of the isotherm. The micropore volume (V_{micro}) was calculated from the t-plot curve at thickness range between 3.5 and 5.4 Å. The micropore size distribution was calculated using the Horvath-Kawazoe (HK) method applying Saito-Foley (SF) correction.

The x-ray photoelectron spectroscopy (XPS) data were collected at the Warwick Photoemission Facility, University of Warwick. The samples investigated in this study were attached to electrically-conductive carbon tape, mounted on to a sample bar and loaded in to a Kratos Axis Ultra DLD spectrometer which possesses a base pressure below 2×10^{-10} mbar. XPS measurements were performed in the main analysis chamber, with the sample being illuminated using a mono chromated Al Kα x-ray source ($h\nu$ = 1486.7 eV). The measurements were conducted at room temperature and at a take-off angle of 90° with respect to the surface parallel. The core level spectra were recorded using a pass energy of 20 eV (resolution approx. 0.4 eV), from an analysis area of 300 µm x 700 µm. The work function and binding energy scale of the spectrometer were calibrated using the Fermi edge and $3d_{5/2}$ peak recorded from a polycrystalline Ag sample prior to the commencement of the experiments. To prevent surface charging, the surface was flooded with a beam of low energy electrons throughout the experiment and this necessitated recalibration of the binding energy scale. To achieve this, the main C-C/C-H component of the C 1*s* spectrum was referenced to 284.8 eV. The data were analysed in the Casa XPS package, using Shirley backgrounds and mixed Gaussian-Lorentzian (Voigt) line shapes. For compositional analysis, the analyser transmission function has been determined using clean metallic foils to determine the detection efficiency across the full binding energy range.

Aluminium, Tin and Ga contents of catalysts were determined by inductively coupled plasma optical emission spectroscopy (ICP-OES). Prior to the measurement the samples were dissolved in an acid mixture of $HF/HNO_3/H_2O$ (1 : 1 : 1).

Scanning Electron Microscopy (SEM) was performed using a ZEISS scanning electron microscope SUPRA 55-VP. The catalysts were coated with gold prior to measurements.

UV–vis diffuse reflectance spectra (DRS) were recorded on a Shimadzu UV-2401 PC spectrometer in diffuse reflectance mode with a 60 mm integrating sphere. $BaSO_4$ was used as the reference. The spectra were transformed into Kubela-Munk function and deconvoluted into subbands by Fityk [45] peak fitting software.

The ^{29}Si solid state magic-angle-spinning, nuclear magnetic resonance (MAS NMR) data were acquired at 7.05 T using a Varian InfinityPlus-300 spectrometer for operating at ^{29}Si and 1H Larmor frequencies (ν_o) of 59.59 and 300.13 MHz, respectively, and a Bruker 7 mm HX probe which enabled MAS frequencies of 5 kHz throughout. The ^{29}Si pulse calibration was undertaken on solid kaolinite from which a π/2 pulse length of 4.5 µs was measured. All ^{29}Si MAS NMR data was measured using single pulse experiments employing π/3 pulse lengths of 3 µs, a recycle delay of 240 s, and high power ^{1}H decoupling of ~80 kHz through the data (FID) acquisition period. The reported ^{29}Si chemical shifts were referenced to TMS (δ_{iso} = 0.0 ppm, IUPAC primary reference) via a secondary solid kaolinite reference (δ_{iso} = -92 ppm). [46] The corresponding ^{27}Al MAS NMR data were measured at 9.4 T using a Bruker Avance HD spectrometer operating at ^{27}Al and ^{1}H Larmor frequencies of 104.23 and 400.13 MHz, respectively, and a Bruker 3.2 mm HX probe which facilitated MAS frequencies of 20 kHz throughout. For quantitative ^{27}Al single pulse measurements within the

central transition to be obtained, a 'non-selective' (solution) π/2 pulse length of 30 μs was calibrated corresponding to a 'selective' (solids) π/12 pulse of 1.67 μs was used in conjunction with a recycle delay of 5 s. The reported ^{27}Al chemical shifts were referenced directly to a 1.1 M Al $(NO_3)_3$ solution (δ_{iso} = 0.0 ppm, IUPAC primary reference). [46]

The ammonia temperature programmed desorption (TPD) were performed by using an excess flow of 2 vol. % ammonia in helium. In a typical experiment, 50 mg of fresh catalyst was loaded in a quartz tube. Prior to measurements catalyst was activated in air flow in-situ at 550 °C for 1 h. Then the catalyst bed was cooled down to at 100 °C and exposed to ammonia for 0.5 h. The ammonia was then desorbed from the catalysts by heating the bed at a rate of 2 °C min^{-1} under helium flow. The amount of ammonia desorbed was measured by using a mass spectrometer (Pfeiffer OmniStar) where m/z = 17, 15 were monitored. Known amount of ammonia was injected by a sample loop for quantification.

In-situ X-ray absorption near edge spectroscopy (XANES) experiments were performed in fluorescence yield, using a silicon drift diode as the detector. The sample was mounted within a helium filled chamber to minimise air absorption, which was especially important for measurements at the Sn edge. [47] A transmission cells designed and built in house are used [48]. The cell can be heated up to 200 °C and it allows uniform mixing of the liquid during the measurements. The liquid was placed between Kapton windows. XANES spectra were collected in transmission mode at the Sn L(III) edge and at Ga K edge at the XMaS beam line of the European Synchrotron Radiation Facility (ESRF) in Grenoble, France. A Si (111) monochromator was used for these experiments. In a typical experiment, 20 mg of catalyst was mixed with 0.2 mL 10 wt. % aqueous glucose solution. Afterwards, this mixture was transferred into the XANES cell and the cell was sealed. The cell was then transferred to the beamline and XANES spectra were recorded at room temperature, after heating to 140 °C, after subsequent heating at 140 °C for 3 h, and after cooling to room temperature. An experiment was carried out without adding sugar by following the same procedure described above. The XANES spectra of references in powder form were recorded at room temperature as self-supporting pellets (13 mm diameter) of the physical mixture of powder materials and the powder crystalline micro cellulose.

2.3. Catalytic activity measurements

Catalytic activity measurements were performed in 4 mL glass reaction vials. The reactors were heated in an oil bath placed on top of a magnetic stirrer. In a typical experiment, a stock solution of D-(+)-Glucose (> 99.5 %, Sigma Aldrich) or of D-(-)-Fructose (> 99 %, Sigma Aldrich) was prepared using the desired solvent at a sugar concentration of 100 mg mL^{-1} and 3 mL was distributed over the reactors. Water, dimethylsulfoxide (DMSO, Fisher Scientific) and 0.1 M hydrochloric acid solution were used as the reaction medium. After introducing the catalyst (40 mg), the reactor was closed and placed in the preheated oil bath at 140 °C for 3 h. Afterwards, the reaction was stopped by quenching the reaction vial at 0 °C. The product mixture was analysed by Shimadzu High Performance Liquid Chromatography (HPLC) equipped with Photo Diode Array (PDA) Detector and Evaporative Light Scattering Detector (ELSD) over a Bio-rad Aminex HPX-87 P column. Glucose, fructose, and mannose were detected by ELSD while HMF was detected by PDA detector. The mobile phase (0.6 mL min^{-1}) was water and the column temperature were 50 °C. Sugars and HMF concentration were calculated with respect to external standards. The conversion was calculated as the number of moles of glucose reacted per mole of glucose in stock solution. The product yield is defined as the number of moles of product formed per mole of glucose in stock solution.

Recycle tests were performed using a 25 mL stainless steel reactor equipped with a PTFE inner lining (Berghof, BR-25). In a typical experiment, a stock solution of D-(+)-Glucose was prepared at a sugar concentration of 100 mg mL^{-1} and 15 mL was added to the reactor along with 200 mg of catalyst. The reactor was then sealed and pressurized to 10 bars using an inert gas (Helium, He) before being immersed into a preheated aluminium heating block on a magnetic stirring plate. After 3 h, the reaction was stopped by quenching the reactor at 0 °C. The catalyst was filtered, washed with deionised water, and dried overnight at 80 °C. The recovered catalyst was used for the subsequent reaction cycle and all the liquids were analysed by HPLC.

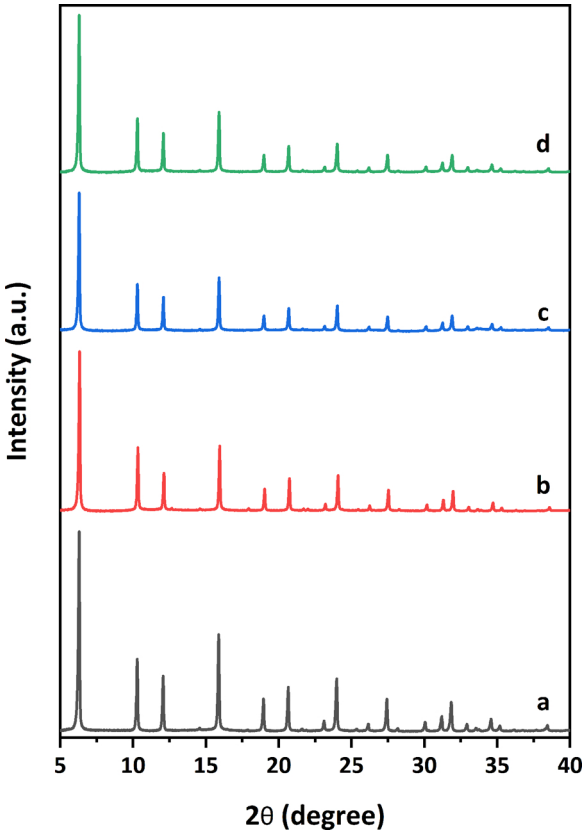

Fig. 1. Powder XRD patterns of catalysts a) HY, b) deAl-HY c) Sn-deAl-HY d) Ga-deAl-HY.

3. Results and discussion

3.1. Structure and morphology

The powder XRD patterns of the catalysts are presented in Fig. 1. The parent material, zeolite Y in hydrogen form, exhibits the typical pattern [49] of a USY zeolite (Fig. 1 a). The dealumination of the parent zeolite Y were conducted in nitric acid prior to the addition of metal precursors. The dealuminated zeolite Y (deAl-HY) exhibits the same intense X-Ray diffraction peaks (Fig. 1 b) indicating that the original structure of HY is retained, and it does not suffer any structural damage from the acid treatment. Fig. 1 c and d show the powder XRD patterns of Sn and Ga incorporated in deAl-HY respectively. Similarly, the powder XRD spectra of these materials exhibit sharp peaks, showing that the zeolite crystal structures are preserved. No features belonging to larger metal oxide phases are observed suggesting the high dispersion of Sn and Ga. This could indicate that Sn and Ga are either embedded into the framework, or the T atoms (Si or Al) of the zeolite framework are partially replaced by the newly introduced metals. It is also possible that they are present in the catalyst as extra framework species in small size (i.e. < 2 nm) outside the detection limits of powder XRD.

Fig. 2 shows the N_2 adsorption-desorption isotherms and the pore

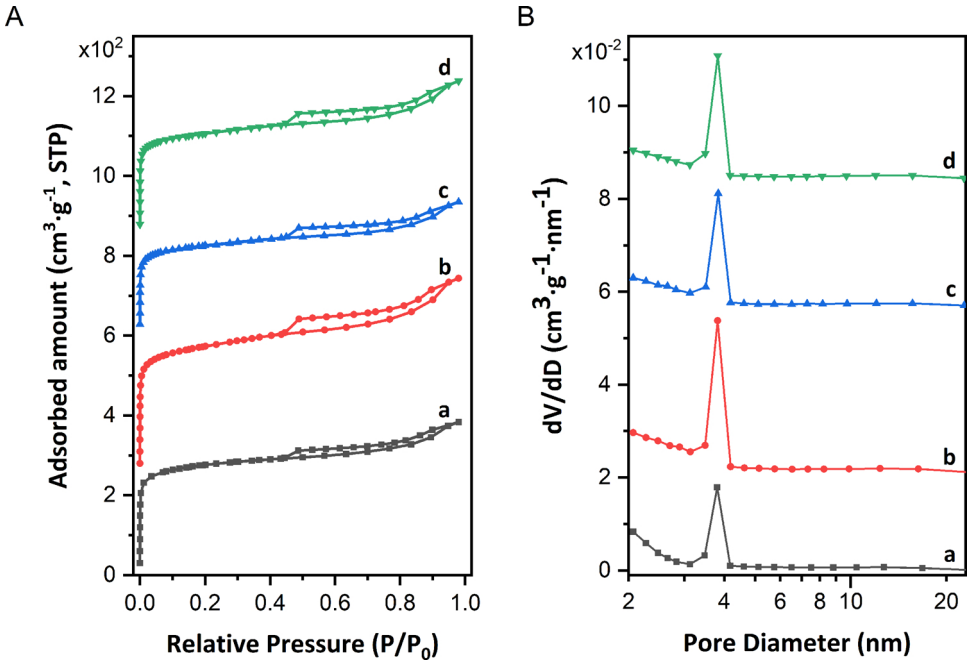

Fig. 2. N_2 physisorption isotherms (A) and pore size distributions (B) of catalysts a) HY, b) deAl-HY c) Sn-deAl-HY d) Ga-deAl-HY.

Table 1
Textural properties of the calcined Y zeolites determined by nitrogen adsorption and acidity obtained from ammonia TPD.

Catalyst	S_{BET} ($m^2\,g^{-1}$)	V_{tot} ($cm^3\,g^{-1}$)	V_{Micro} ($cm^3\,g^{-1}$)	V_{Meso} ($cm^3\,g^{-1}$)	Acid sites from NH_3-TPD (mmol g^{-1})				
					T(°C)	Weak	T(°C)	Strong	Total
HY	987	0.44	0.31	0.13	190	0.144	372	0.304	0.447
deAl-HY	1155	0.56	0.33	0.23	400	0.002	555	0.001	0.003
Sn-deAl-HY	807	0.38	0.24	0.14	190	0.004	266	0.007	0.012
Ga-deAl-HY	917	0.44	0.27	0.17	315	0.005	503	0.025	0.030

size distributions of the catalysts. The corresponding textural properties are summarised in Table 1. The physisorption isotherms (Fig. 2 A) show type IV isotherms with H4 type hysteresis loops for all materials, which is typical of microporous materials with the presence of mesoporosity. In all isotherms a steep rise is observed at the low relative pressures ($P/P_0 < 0.05$) which evidences the microporous structure of the zeolites. A hysteresis is visible in all catalysts above relative pressures of $P/P_0 > 0.4$. The hysteresis is very narrow in the parent zeolite Y, conversely, it is wider in dealuminated sample (Fig. 2 A b). The Sn and Ga incorporated catalysts show hysteresis narrower than the dealuminated catalyst, and wider than the parent zeolite Y material. This shows that mesopores are present in the parent material (HY), and more mesopores are generated by dealumination by acid treatment. It is common that the acid treatment of zeolites results in the formation of mesopores [50]. The dealuminated catalyst has a larger mesopore volume (V_{meso}) and total volume (V_{tot}) than the parent HY zeolite and a similar micropore volume (V_{mic}) to the parent HY zeolite (Table 1). The addition of Sn and Ga in dealuminated zeolite Y (deAl-HY) resulted in the decrease of mesopore and micropore volume, which is usually observed in post-treatment of zeolites and porous silicas. This could be due to the occupation of the pores with the metals. The pore size distributions of the catalysts show a narrow distribution in the mesoporous range, peaking around 3.8 nm for all catalysts (Fig. 2 B).

The acidity obtained from the deconvolution of the NH_3-TPD profiles of catalysts are given in Table 1. Each NH_3-TPD curve (Fig. 3) exhibited two main types of NH_3 desorption, named as weak and strong peaks, corresponding to low and high mean desorption temperature, respectively. The dealumination of HY zeolite resulted in a decrease of acid sites, which could be due to the removal of aluminium both extra framework and framework. On the other hand, the NH_3 desorption peaks shifted significantly to higher temperatures, showing the increase in acid strength. This is expected because the remaining Al in the catalyst could become more isolated and therefore forms the stronger acidic isolated Si-O-Al linkages which is the origin of acidity in zeolites. The addition of Sn reduced the acid strength of the material, however the total acidity increased, implying the introduction of Lewis acid sides due to the addition of Sn. Conversely, Ga addition endured the acid strength of parent deAl-HY catalyst relatively high, and doubled the total acidity as compared to Sn addition.

Solid state ^{27}Al and ^{29}Si MAS NMR measurements were performed and deconvoluted (Fig. 4). The Al and Si species and their relative intensities are given in Table 2. Three different Al sites are apparent in each sample in varying quantities. As has been previously reported, these sites can be attributed to tetrahedrally coordinated Al in the zeolite framework located ~60 ppm and octahedrally coordinated extra-framework Al located at both ~6 and ~30 ppm [51]. The spectra of HY (Fig. 4 a) indicates that ~70 % of Al has a tetrahedral geometry signifying that the vast majority of Al present is in the zeolite framework as a silica-alumina phase. Upon dealumination (Fig. 4 b), a significant reduction in tetrahedral Al (~9%) is observed implying that the dealumination removed most of the aluminium from the framework in deAl-HY. The incorporation of Sn and Ga in the dealuminated zeolite leads to a larger proportion of Al in the structure when compared to deAl-HY. Greater short-range disorder is also observed due to the apparent broader line shapes. The ^{29}Si MAS NMR shows that the most prominent Si sites in all catalysts is Q^4 at ~108 ppm, defined by the

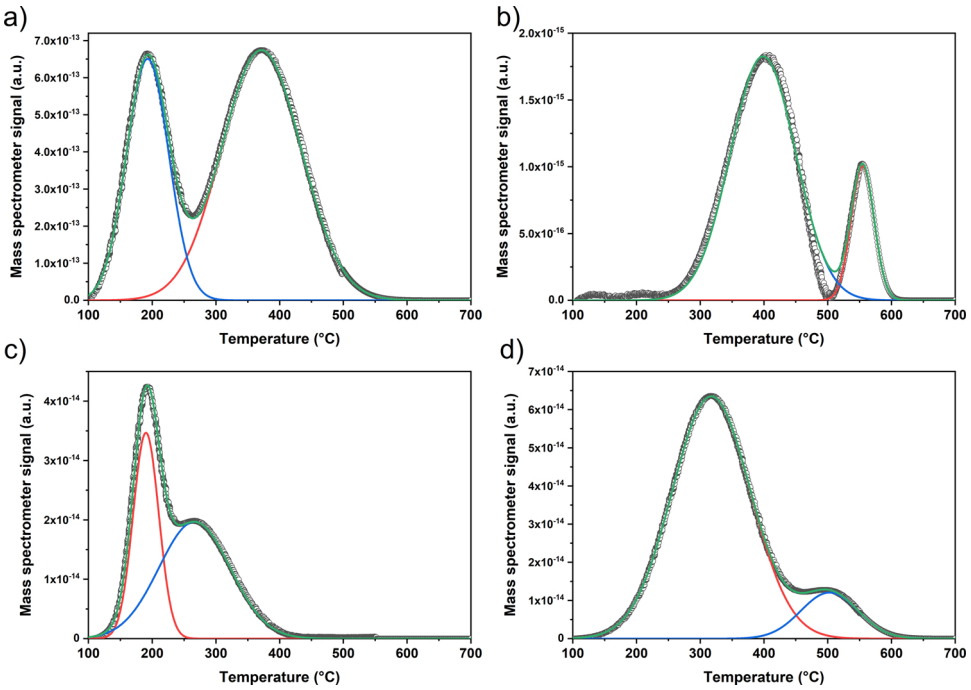

Fig. 3. NH_3-TPD profiles of a) HY, b) DeAl-HY c) Sn-deAl-HY d) Ga-deAl-HY.

speciation Q^n: $Si(OSi)_nOR_{(4-n)}$ (with R = Al or H). The introduction of metal species into the deAl-HY framework results in a decrease in the relative amount of Q^3 at ~103 ppm when compared to the base zeolite. This is caused by the removal of −OH groups in the silica network via replacement by Sn or Ga; thus, showing the incorporation of Sn and Ga into the zeolite framework. This indicates a higher network connectivity in the dealuminated zeolites with Sn and Ga incorporation.

The elemental compositions of the catalysts are listed in Table 3. Quantifying the aluminium content of HY reveals a silicon to aluminium (Si/Al) ratio of 19. The subsequent dealumination effectively removed most of the aluminium from the parent HY material ultimately resulting in a Si/Al ratio of 160. These relatively low Al content is ideal for the Y zeolites to be employed for glucose conversion in water. When more aluminium is extracted the number of acid sites are reduced. On the other hand, the remaining acid sites are more isolated and thus result in an increase in the acid strength of the sites. The introduction of metal species into the deAl-HY framework yielded catalysts with Sn and Ga contents of 2.9 wt. % and 2.3 wt. % respectively. These correspond to molar Si/Sn and Si/Ga ratios of 65 and 48 for the tin and gallium containing materials, respectively.

The states of Sn and Ga in Sn-deAl-HY and Ga-deAl-HY are investigated by XPS (Fig. 5). In the Sn 3*d* region, two signals are revealed at 487.4 and 495.8 eV. These peaks are assigned to $3d_{5/2}$ and $3d_{3/2}$ photoelectrons of tetrahedrally coordinated framework Sn species respectively [52]. The binding energies of octahedral Sn species specific to SnO_2 are usually assigned to 486.0 and 494.4 eV [53]. The clear sharp tetrahedral peaks in the absence of any octahedral peaks in XPS spectra of Sn-deAl-HY indicates that Sn is mostly tetrahedrally

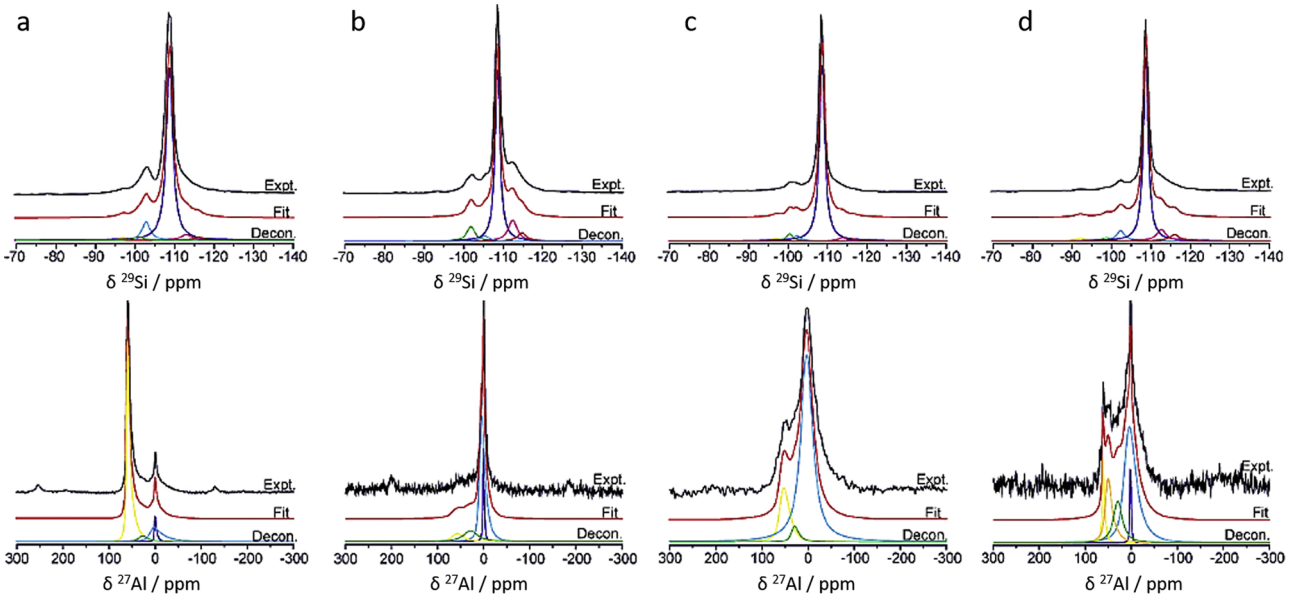

Fig. 4. ^{29}Si (above) and ^{27}Al (below) MAS NMR of the catalysts; a) HY, b) deAl-HY c) Sn-deAl-HY d) Ga-deAl-HY. The experimental data (black line) the fit (red line) and the deconvolution peaks are presented (For interpretation of the references to colour in this figure legend, the reader is referred to the web version of this article).

Table 2
Chemical shifts and intensities of Si and Al sites obtained from ^{29}Si and ^{27}Al MAS NMR.

Catalyst	AlO_4 (ppm)	AlO_5 (ppm)	AlO_6 (ppm)	Si (Q^2) (ppm)	Si (Q^3) (ppm)	Si (Q^4) (ppm)
HY	61.4 (69.8 %)	29.1 (6.3 %)	1.2, 6.0 (23.9 %)	−96.9 (1.8 %)	−100.9, -102.8 (12.6 %)	−108.7, -113.0 (85.6 %)
deAl-HY	61.2 (8.6 %)	29.6 (16.1 %)	1.3, 6.0 (75.3 %)	−93.4 (0.2 %)	−101.8, -105.4 (13.1 %)	−108.6, -112.4 (86.7 %)
Sn-deAl-HY	61.5 (16.5 %)	32.2 (3.8 %)	6.9 (79.7 %)	−97.0 (1.6 %)	−100.4, -102.2 (7.4 %)	−108.6, -113.8 (91 %)
Ga-deAl-HY	62.4, 52.8 (25.7 %)	31.7 (16.2 %)	2.5, 8.7 (58.1 %)	−92.1 (1.9 %)	−98.8, -102.3 (9.2 %)	−108.7, -112.6 (88.9 %)

Table 3
Elemental composition of catalysts and molar metal ratios obtained from elemental analysis.

Catalyst	Al (wt. %)	Sn (wt. %)	Ga (wt. %)	Si/Al	Si/Sn	Si/Ga
HY	2.3	n/a	n/a	19	n/a	n/a
deAl-HY	0.28	n/a	n/a	160	n/a	n/a
Sn-deAl-HY	0.26	2.9	n/a	164	65 (31[a])	n/a
Ga-deAl-HY	0.28	n/a	2.3	152	n/a	48 (43[a])

[a] Obtained from XPS, given here for comparison. The atomic content of catalysts obtained by XPS is provided in Supplementary information, Table S1.

coordinated in the zeolite Y framework. Fig. 5 b shows the Ga $2p_{3/2}$ XPS spectra of the Ga-deAl-HY catalyst. The XPS spectra was fitted by two peaks showing binding energy values centred at 1119.2 and 1120.8 eV. These could be attributed to framework and extra-framework Ga species respectively [54]. The relative intensities of these peaks are 79 % and 21 %, which indicates that most of the Ga species are in the zeolitic framework. Si/Ga ratio obtained by elemental analysis (Si/Ga = 48) is close to the ratio obtained by XPS (Si/Ga = 43), inferring that the Ga species are dispersed close to surface. On the other hand, Sn species are most likely to be dispersed all around the zeolite framework, where roughly half of them are detectable by XPS. The aluminium atom is observed clearly only in HY zeolite by XPS (Supporting information, Table S1) and all the other catalysts do not exhibit detectable amounts as expected after the dealumination treatment of the parent HY.

Scanning electron microscopy (SEM) images of the catalysts are given in Fig. 6. The morphologies of the parent HY zeolite, deAl-HY and Sn and Ga doped catalysts are similar with particle sizes in the range

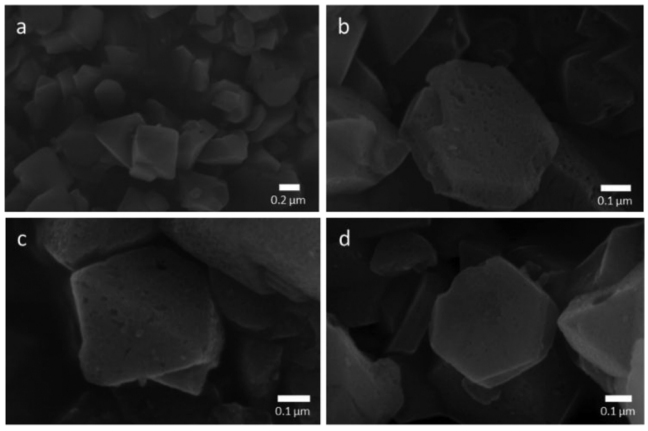

Fig. 6. SEM images of catalysts; a) HY, b) deAl-HY c) Sn-deAl-HY d) Ga-deAl-HY.

between 0.1 and 0.5 microns. These similar images show that the dealumination and metal doping does not adversely affect the crystallinity of the parent zeolite Y in line with the XRD results. The modified catalysts contain polygonal crystals. The rougher outer surfaces are clearly visible which implies the increase of defect sites. No clear mesopores can be distinguished from SEM images. The zeolite particles are made up of crystals in varying sizes arranged into larger aggregates. This could lead to disordered mesoporosity dispersed inside and all around the zeolite crystals.

UV–vis diffuse reflectance spectra of the catalysts are shown in

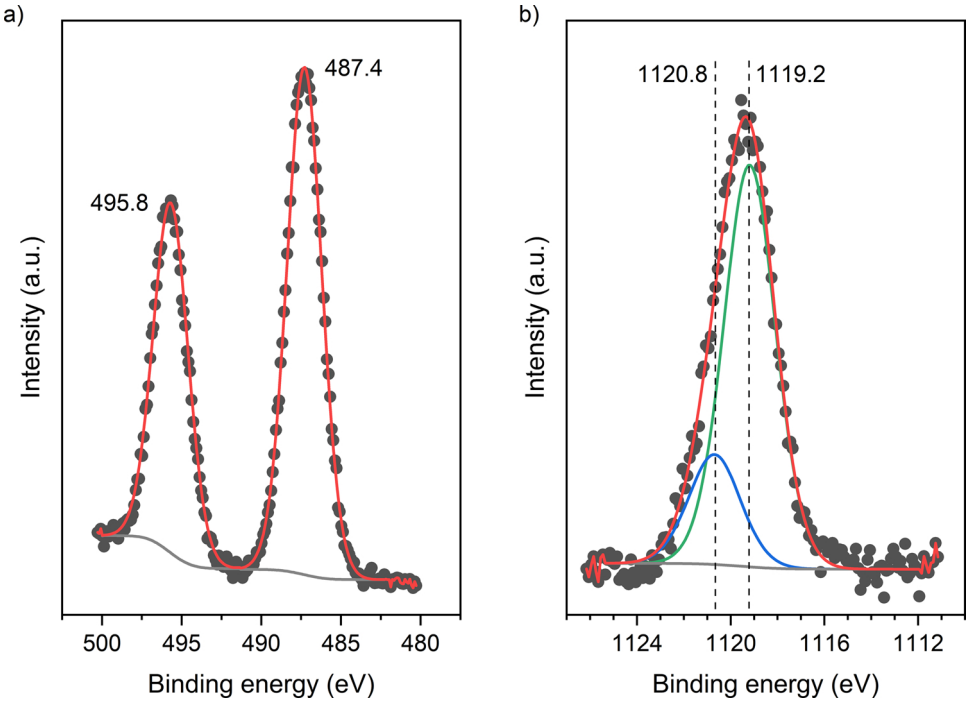

Fig. 5. X-Ray Photoelectron Spectroscopy (XPS) of a) the Sn 3*d* region of Sn-deAl-HY b) the Ga $2p_{3/2}$ region of Ga-deAl-HY.

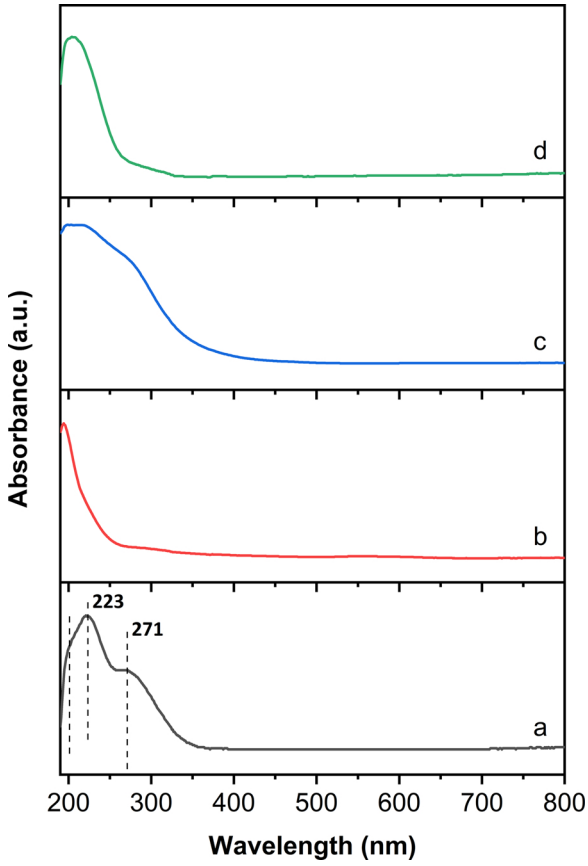

Fig. 7. UV–vis diffuse reflectance spectra of catalysts a) HY, b) deAl-HY c) Sn-deAl-HY d) Ga-deAl-HY.

Fig. 7 and their deconvoluted counterparts are presented in supporting information (Supporting information, Figure S1). The spectrum of HY (Fig. 7 a) is dominated by two intense bands at 223 nm with a shoulder at 201 nm and 271 nm, which are typical of zeolite framework [55,56]. Dealumination of the parent zeolite Y resulted in a change in the relative intensities of the features; the band at 201 nm became the sharpest peak (Fig. 7 b). The lower wavelengths are usually ascribed to the charge transfer between the oxygens and the tetrahedrally coordinated framework metal atoms. This implies that the dealumination process might have washed out the extra framework alumina and caused a higher absorption in lower wavelengths. The introduction of Sn to deAl-HY results in a broader spectrum with bands between 200 nm and 300 nm (Fig. 7 c). This UV–vis spectra of Sn-deAl-HY is typical of conventional Sn containing zeolites, and the broad absorption at a maximum around 270 nm with a shoulder expanding to 300 nm is previously ascribed to extra framework or polymeric Sn-O-Sn type sites, while the peak at 220 nm is often assumed to be the catalytically active isolated Sn^{IV} in tetrahedral coordination in the framework. [57] The absence of strong absorption above 300 nm indicates that there is no bulk SnO_2 present because SnO_2 usually shows an absorption band at 340 nm that could be attributed to the octahedral coordination of Sn in the SnO_2 framework. [58] Conversely, Ga-deAl-HY shows a narrower spectrum, maximising at 205 nm with a shoulder until 270 nm. This may indicate that the Ga is occupying mostly the framework positions as isolated species and therefore its spectrum is dominated with the peak at 205 nm, whereas Sn has a broader distribution between the framework and extra framework sites.

3.2. Glucose dehydration to HMF

Fig. 8 a–c shows the conversion of glucose and the product yields of HMF, fructose and mannose in water, in acid solution (HCl, pH = 1.0) and in a polar aprotic solvent (DMSO) respectively. The blank reaction without any catalyst results in a glucose conversion like that of HY in water (Fig. 8 a). It is evident that HY does not have any significant effect on the reaction. This is likely due to the lack of Lewis acid sites in HY. The deAl-HY shows similar results to HY and blank reactions, in other words, the deAl-HY zeolite does not catalyse the reaction any further than HY. When the Sn is incorporated into the zeolite Y framework, more drastic changes are observed in conversion and in product yields. The catalyst Sn-deAl-HY zeolite resulted in a glucose conversion of 35 %. More interestingly, the fructose yield of 13 % was observed. This shows that Sn included zeolite Y is an active catalyst for the isomerization of glucose into fructose. The isolated framework Sn^{IV} species are considered the active sites for the isomerization reaction over Sn-beta in literature [24], thus this result indicates that Sn is incorporated as isolated species into the framework of deAl-HY. Similarly, the Ga-deAl-HY shows activity for isomerization of glucose into fructose. The glucose conversion (17 %) and fructose yield (5 %) were lower than the Sn included catalyst. Nevertheless, this activity proves that the Ga species form isolated active sites in Ga-deAl-HY and they provide the Lewis acidity necessary to catalyse the isomerization reaction.

It has been shown in literature that the fructose could be easily converted into HMF in mineral acids at pH = 1.0 (0.1 M HCl) catalysed by the Brønsted acidity. [59] To drive the reaction towards HMF, we examined the glucose conversion over the catalysts in 0.1 M HCl (Fig. 8 b). The glucose conversion increased in the blank reaction and over all catalysts at pH = 1.0 in the Brønsted acidic medium. The HY shows slightly higher glucose conversion and HMF yields than the blank reaction, whereas deAl-HY and Sn-deAl-HY show similar results to blank reaction. The conversion over Sn-deAl-HY in 0.1 M HCl is not significantly different as compared to when water is the reaction medium over the same catalyst. As the mechanism of glucose conversion could be quite complex [60], in the presence of HCl the reaction may proceed through the routes catalysed by the mineral acid only in a competitive fashion and the Sn-deAl-HY may not be able to play a role. On the other hand, Ga-deAl-HY shows higher glucose conversion than all the other cases. Although the reason is not clear, it could be due to the active Ga species catalysing the glucose and any other reaction intermediates effectively not only to form HMF but to form unidentified side products through alternative reaction pathways. No fructose formation is observed over Sn-deAl-HY and trace amount were seen over Ga-deAl-HY (< 2 %). This implies that the reaction is mainly catalysed by the Brønsted acidic protons of the mineral acid where all the fructose formed is readily converted into HMF (or into any other side product). It is important to note that HMF does not necessarily need to be formed through the isomerisation of glucose to fructose catalysed by the zeolites under these conditions. In other words, it is possible that HMF could also be formed through Brønsted acidic proton catalysing alternative reaction mechanisms. The alternative reaction pathways could be prevalent under these conditions, and we speculate that it could be the reason for HY showing higher glucose conversion than deAl-HY where the former has higher alumina content, and thus possesses more acid sites.

The widely accepted mechanism of glucose isomerisation to fructose through hydride shift is given in Scheme 1. The other products include mannose through glucose epimerisation, soluble polymers and insoluble poorly characterised oligomeric species named as humins. The aprotic polar solvents, i.e. DMSO, was shown to supress the formation of humins (carbon based dark-coloured tarry solids [61]) and enhance HMF yields [62]. Not only are humins an undesired side product, but also their accumulation may block the catalytically actives sites. DMSO has also been shown to catalyse the fructose dehydration to HMF [63]. Therefore, the effect of DMSO on reactions is twofold. As shown in Fig. 8 c, the use of DMSO as the solvent significantly increased glucose conversion in the blank reaction and in the presence of all catalysts. The

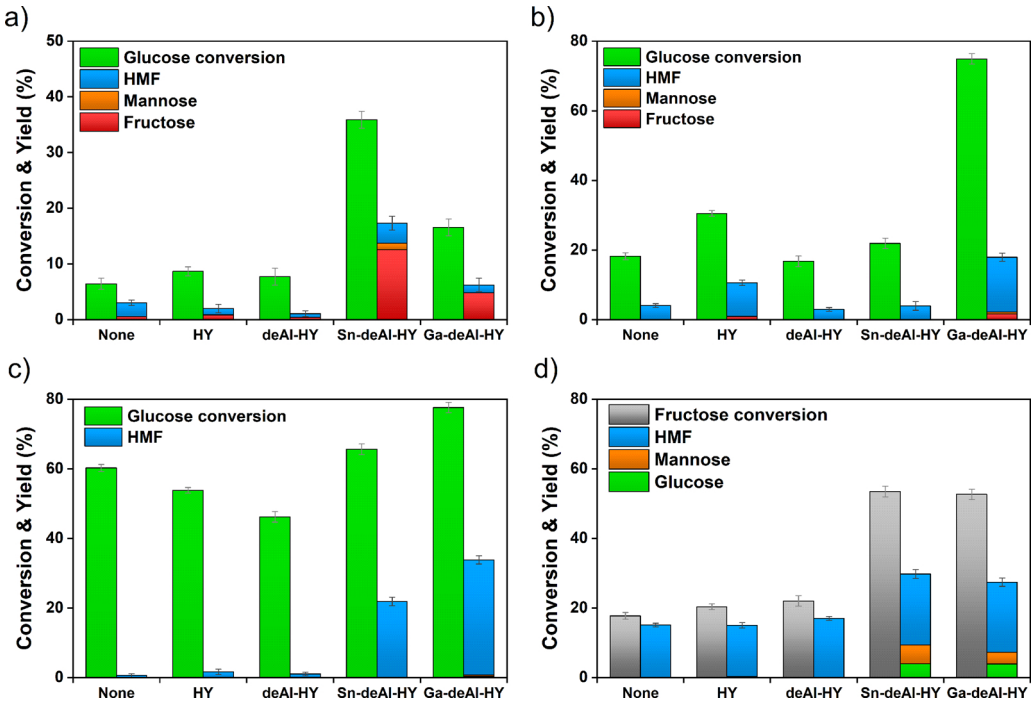

Fig. 8. Glucose conversion and product yields over catalysts in a) water, b) 0.1 M HCl and c) DMSO. d) Fructose conversion and product yield over catalysts in water. Reactions were performed at 140 °C for 3 h starting with a stock solution of 10 wt. % glucose.

blank reaction, HY and deAl-HY lead to the formation of only trace amounts of fructose, mannose and HMF. Conversely, the use of Sn-deAl-HY in DMSO resulted in an HMF yield of 22 %, higher than that produced in either water or HCl over the same catalyst. No fructose was observed, which implies that the dehydration of fructose to HMF is faster than the glucose isomerization to fructose. Ga-deAl-HY lead to an even a higher conversion of glucose 78 % accompanied with a 33 % HMF yield. Neither fructose nor mannose was observed over Sn-deAl-HY and only trace amounts of mannose and fructose was observed over Ga-deAl-HY. Sn-beta is the most studied catalyst, and thus it could be considered a benchmark catalyst for glucose isomerisation. It shows 54 % glucose conversion with 30 % fructose and 9% mannose yield under similar conditions used in this study and no HMF formation was reported [10]. Therefore, the 33 % HMF yield over Ga-deAl-HY obtained in a single pot is quite promising. The product selectivity towards HMF over Sn-deAl-HY and Ga-deAl-HY makes the DMSO as a noticeable reaction medium. Nevertheless, DMSO rather remains industrially undesirable, and water is the preferred reaction medium as it is the greenest solvent.

Fructose can readily be converted to HMF and therefore the initial isomerisation step is usually accepted as the rate limiting step in glucose utilisation. Therefore, we studied fructose conversion in water under the same conditions over catalysts. Fig. 8 d shows that the blank reaction, HY and deAl-HY lead to a fructose conversion of around 20 %. The HMF yields were around 15 % which makes the selectivity towards HMF considerably high. The fructose dehydration to HMF could be catalysed by Brønsted acid or Lewis acid catalysts and could also be autocatalytic. [64] Nonetheless, HY and deAl-HY do not show particularly higher conversion than in the case where no catalyst is present (blank reaction). Conversely, both the tin and gallium containing catalysts show fructose conversion of around 53 %, a significant increase when compared to the other cases. The resulting HMF yields are also higher (20 %). The fructose conversion is significantly higher than the glucose conversion in water. But, the HMF formation is accompanied by the formation of unknown side products. This implies that side products in glucose reactions might have been formed from not only glucose, but also fructose or HMF itself. The Sn-deAl-HY and Ga-deAl-HY zeolites also resulted in the production of glucose and mannose. This implies

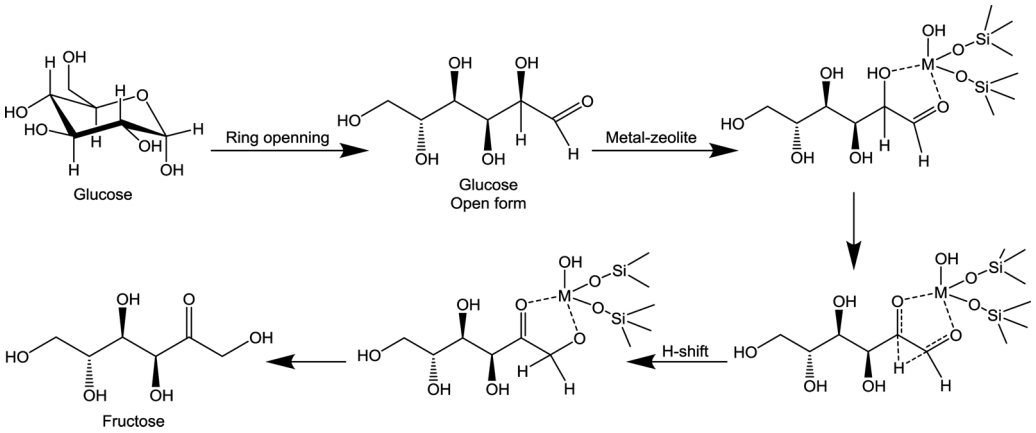

Scheme 1. The reaction mechanism of glucose isomerisation over Lewis acid metal doped zeolites.

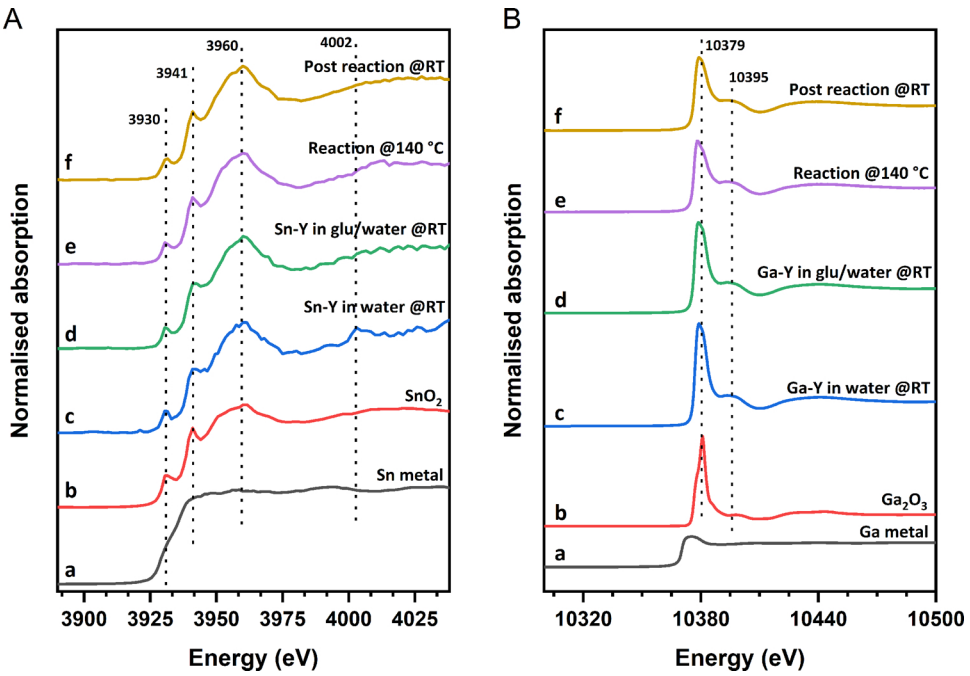

Fig. 9. XANES of Sn-deAl-HY (A) and Ga-deAl-HY (B). The spectra of metal foil (a) and metal oxide (b) are given as reference. The spectra were taken at c) catalyst in water at room temperature, d) catalyst in 10 wt. % glucose stock solution at room temperature, e) after 3 h of reaction at 140 °C, and f) post reaction after cooling down the reactor to room temperature. Sn-deAl-HY is shortened as Sn-Y and Ga-deAl-HY is shortened as Ga-Y on the figures. RT represents room temperature. Glu/water represents the solution of 10 wt. % glucose in water.

that the initial isomerisation and epimerisation steps are equilibrium reactions. Therefore, biphasic systems may work best for increasing glucose conversion and for increasing HMF yields by continual removal HMF.

We performed XANES analysis in-situ at the Sn L_{III}-edge and Ga K-edge to reveal the changes in the chemical environment of the active metal sites during the reaction in water (Fig. 9). First, the spectra were collected when the catalysts were in water in the absence of glucose at room temperature. Later catalysts were added in 10 wt. % glucose stock solution in water and scans were collected similarly at room temperature when there is no reaction was taking place. The XANES spectra of Sn-deAl-HY revealed bands at 3930 eV, 3941 eV and 3960 eV. These are typical features of tin oxide and the XANES spectra of Sn-deAl-HY which mostly resemble Sn oxide. The only difference is that the band at 3941 eV is relatively less sharp. This could be due to the presence of isolated Sn^{IV} species in the zeolite framework. The presence of glucose in water at room temperature has not affected the position of these features. A post edge band was also observed at 4002 eV in the case of Sn-deAl-HY in water and it disappears with the presence of glucose in solution. Afterwards, the reactor was heated to the reaction temperature of 140 °C and the spectra were collected in situ at 140 °C after 10 min and after 3 h. The band at 3941 eV became sharper relative to other bands as soon as the reaction started when compared to the no reaction case (Fig. 9A d–e). It remained the same and similar spectra were obtained after 3 h of reaction. Meanwhile, there were no changes in other features. The pre-edge features in XANES are very sensitive to the oxidation state and chemical environment of the metal under study. In this case, the change in the sharpness of the band at 3941 eV could be due to the isolated Sn sites being coordinated with the oxygens of the reactants and intermediates, i.e. glucose, fructose, and HMF. Similar trends are observed in the case of Ga-deAl-HY (Fig. 9B). The two main features of the XANES spectra of Ga are at 10,379 eV and 10,395 eV. The spectra of Ga-deAl-HY resembles that of Ga oxide. Upon addition of glucose in water, the spectra do not have any difference to that of Ga-deAl-HY in water. However, the reaction affects the relative intensity of these bands, and the latter band becomes relatively more intense. Likewise, it could be due to the strong interaction of the isolated Ga species with the reacting hydrocarbon molecules in the solution medium.

3.3. Catalyst stability and recycling

The deactivation of the catalysts usually occurs through the leaching of the active metal species during the reaction. Therefore, we studied the stability of the catalysts by analysing the amount of active metals (Sn or Ga) in the reaction medium after the reaction, the results of which are shown in Table 4. Sn-deAl-HY shows higher stability as compared to Ga-deAl-HY in all solvents. The amount of tin leached from Sn-deAl-HY is less than 0.6 % of Sn present in the catalyst in the beginning of the reaction in all solvents. In contrast, Ga leached in greater amounts particularly at pH = 1.0. The amount of Ga leached in 0.1 M HCl is as high as 55 %.

To assess the reusability of the materials, recycle reactions were performed. The Sn-deAl-HY was recycled a total of four times in water and in DMSO. After each recycle reaction the catalyst was recovered via a centrifuge before being added back to a fresh stock solution. As shown in Fig. 10, the activity of Sn-deAl-HY significantly reduced from first to second cycle of reaction and remained constant thereafter in the following reaction cycles. Given the trace amount Sn metal in reaction solvent, we concluded that leaching is not the main reason for the deactivation of Sn-deAl-HY. Instead the deactivation could be due to an accumulation of humins on the catalyst surface and thus blocking the access to the active sites over time. To remove humin deposits, recycled Sn-deAl-HY was reactivated by calcination at elevated temperature (550 °C) after the fourth cycle. XRD analysis revealed that the zeolite Y structure is maintained after reactivation by calcination (Supporting information, Figure S2). Nevertheless, the performance of the catalyst was not recovered. In another attempt, the Sn-deAl-HY was regenerated after the 1st reaction cycle. Similarly, this did not help to recover its

Table 4
Tin and Gallium content of the post reaction solution after 3 h at 140 °C.

Catalyst	Medium	Sn (ppm)	Ga (ppm)
Sn-deAl-H-Y	Water	2.1	n/a
Sn-deAl-H-Y	HCl (pH = 1.0)	0.4	n/a
Sn-deAl-H-Y	DMSO	0.5	n/a
Ga-deAl-H-Y	Water	n/a	32.1
Ga-deAl-H-Y	HCl (pH = 1.0)	n/a	167.2
Ga-deAl-H-Y	DMSO	n/a	40.7

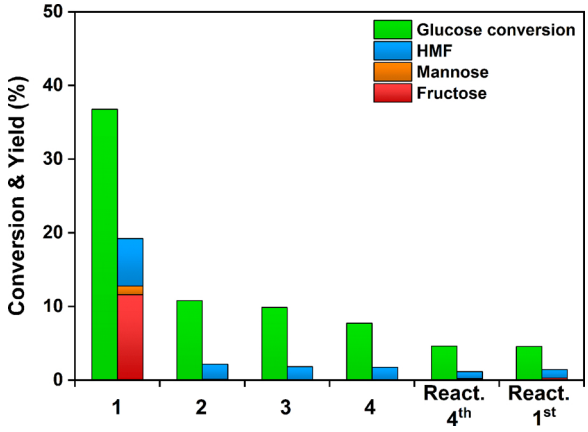

Fig. 10. Recycling of Sn-deAl-HY in water. Glucose conversion and product yields of 4 reaction cycles and after the reactivation of the catalyst following 4th and 1st cycle. Reactions were performed at 140 °C for 3 h starting with a stock solution of 10 wt. % glucose.

activity either.

Fig. 11 shows the recycling of Sn-deAl-HY and Ga-deAl-HY in DMSO. Glucose conversion and HMF yields remain stable over the recycles, within ± 10 %. A slight decrease is observed after 3rd cycle and this decline is far less severe than that observed in the water. The reactivation of the Sn-deAl-HY was found to effectively recover the activity of the catalyst after this cycle. The conversion of glucose and HMF yields over Ga-deAl-HY showed a similar trend and the calcination of the spent Ga-deAl-HY in air recovered catalytic activity effectively (Fig. 11 b). XRD analysis of both Sn-deAl-HY and Ga-deAl-HY after reactivation (Supporting information, Figure S3) show that the structures of the zeolites have been preserved.

4. Conclusions

Tin and gallium containing zeolite Y materials effectively catalyse the isomerization of glucose to fructose and HMF production in water, 0.1 M HCl and DMSO. The catalysts can be produced using a simple and scalable method that utilises commercially available zeolite Y. Of the materials considered, Sn-deAl-HY was found to be the most active material for glucose isomerization in water. Meanwhile, Ga-deAl-HY was shown to generate the highest activity and HMF yield when reactions were conducted in DMSO. Both catalysts showed higher selectivity towards HMF in DMSO. We concluded that the deactivation of Sn-deAl-HY in water was likely a result of humin accumulation on the catalyst rather than leaching. Whereas, Ga leaches out significantly in water. Both Sn-deAl-HY and Ga-deAl-HY showed stable catalytic performance in cycles of reactions conducted in DMSO. Both catalysts are selective and can be regenerated when reactions are conducted in DMSO. This makes them promising catalysts for glucose utilisation. Overall, we showed that post synthesis modification of zeolite Y, and the use of Ga as active metal in zeolite Y, may offer an attractive route towards the production of HMF in bio renewables industry.

CRediT authorship contribution statement

Ryan Oozeerally: Investigation, Writing - original draft, Formal analysis, Methodology, Writing - review & editing. **John Pillier:** Resources, Methodology, Investigation. **Emre Kilic:** Investigation, Software. **Paul B.J. Thompson:** Resources, Methodology, Investigation, Software, Data curation, Writing - review & editing. **Marc Walker:** Data curation, Writing - review & editing, Resources. **Benjamin E. Griffith:** Data curation, Investigation, Writing - review & editing. **John V. Hanna:** Resources, Supervision, Funding acquisition, Writing - review & editing. **Volkan Degirmenci:** Conceptualization, Methodology, Writing - original draft, Visualization, Supervision, Funding acquisition, Writing - review & editing.

Declaration of Competing Interest

The authors report no declarations of interest.

Acknowledgements

The XANES experiments were performed on beamline BM28 XMaS at the European Synchrotron Radiation Facility (ESRF), Grenoble, France. XMaS is a UK national research facility supported by EPSRC. We are grateful to all the beamline team staff for their support. V.D and E.K. are grateful for the support provided by Royal Academy of Engineering under the grant number NRCP1617/6/204. J.V.H. acknowledges

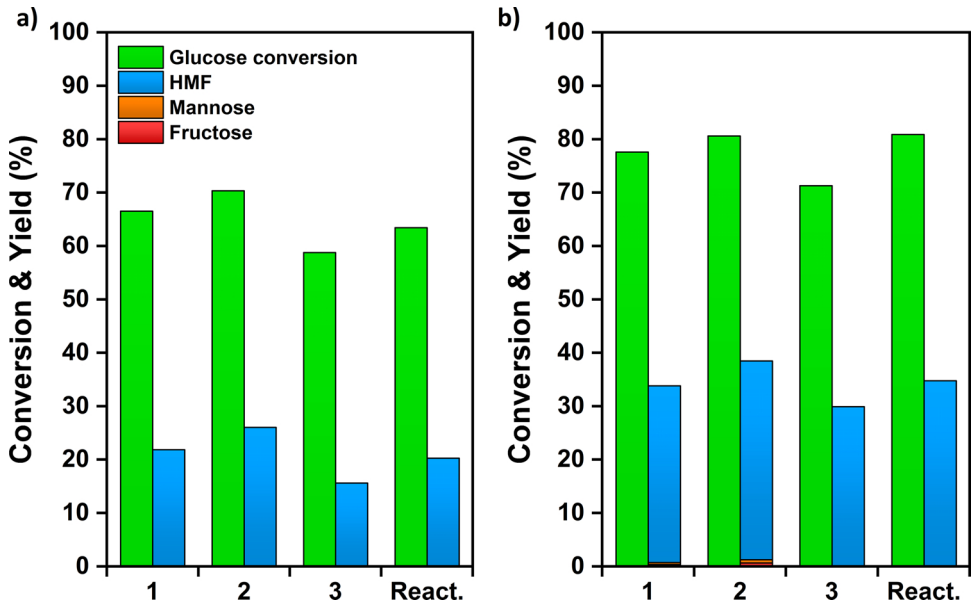

Fig. 11. Recycling of a) Sn-deAl-HY and b) Ga-deAl-HY in DMSO. Glucose conversion and product yields of 3 reaction cycles and after the reactivation of the catalysts following the 3rd cycle. Reactions were performed at 140 °C for 3 h starting with a stock solution of 10 wt. % glucose.

financial support for the solid state NMR instrumentation at Warwick used in this research which was funded by EPSRC (grants EP/M028186/1 and EP/K024418/1), the University of Warwick, and the Birmingham Science City AM1 and AM2 projects which were supported by Advantage West Midlands (AWM) and the European Regional Development Fund (ERDF). Authors thank to Nikolay Cherkasov for his support on TPD experiments.

Appendix A. Supplementary data

Supplementary material related to this article can be found, in the online version, at doi:https://doi.org/10.1016/j.apcata.2020.117798.

References

[1] A. Mukherjee, M.Je. Dumont, V. Raghavan, Biomass Bioenerg. 72 (2015) 143–183.
[2] F.A. Kucherov, L.V. Romashov, K.I. Galkin, V.P. Ananikov, ACS Sustain. Chem. Eng. 6 (2018) 8064–8092.
[3] I.K.M. Yu, D.C.W. Tsang, Bioresour. Technol. 238 (2017) 716–732.
[4] R.J. Van Putten, J.C. Van Der Waal, E. De Jong, C.B. Rasrendra, H.J. Heeres, J.G. De Vries, Chem. Rev. 113 (2013) 1499–1597.
[5] J.N. Chheda, Y. Roman-Leshkov, J.A. Dumesic, Green Chem. 9 (2007) 342–350.
[6] Y. Roman-Leshkov, J.N. Chheda, J.A. Dumesic, Science 312 (2006) 1933–1937.
[7] V. Degirmenci, E.J.M. Hensen, Environ. Prog. Sustain. Energy 33 (2014) 657–662.
[8] V. Degirmenci, E.A. Pidko, P.C.M.M. Magusin, E.J.M. Hensen, ChemCatChem 3 (2011) 969–972.
[9] S.G. Wettstein, D.M. Alonso, E.I. Gürbüz, J.A. Dumesic, Curr. Opin. Chem. Eng. 1 (2012) 218–224.
[10] M. Moliner, Y. Román-Leshkov, M.E. Davis, Proc. Natl. Acad. Sci. U.S.A. 107 (2010) 6164.
[11] G.M. Lari, P.Y. Dapsens, D. Scholz, S. Mitchell, C. Mondelli, J. Pérez-Ramírez, Green Chem. 18 (2016) 1249–1260.
[12] D. Padovan, C. Parsons, M. Simplicio Grasina, C. Hammond, Green Chem. 18 (2016) 5041–5049.
[13] E. Nikolla, Y. Román-Leshkov, M. Moliner, M.E. Davis, ACS Catal. 1 (2011) 408–410.
[14] R. Bermejo-Deval, R.S. Assary, E. Nikolla, M. Moliner, Y. Román-Leshkov, S.-J. Hwang, A. Palsdottir, D. Silverman, R.F. Lobo, L.A. Curtiss, M.E. Davis, Proc. Natl. Acad. Sci. U. S. A. 109 (2012) 9727.
[15] J.S. Kruger, V. Choudhary, V. Nikolakis, D.G. Vlachos, ACS Catal. 3 (2013) 1279–1291.
[16] J. Zhang, L. Wang, G. Wang, F. Chen, J. Zhu, C. Wang, C. Bian, S. Pan, F.-S. Xiao, ACS Sustain. Chem. Eng. 5 (2017) 3123–3131.
[17] L. Ren, Q. Guo, P. Kumar, M. Orazov, D. Xu, S.M. Alhassan, K.A. Mkhoyan, M.E. Davis, M. Tsapatsis, Angew. Chem. Int. Ed. 54 (2015) 10848–10851.
[18] P.Y. Dapsens, C. Mondelli, J. Jagielski, R. Hauert, J. Pérez-Ramírez, Catal. Sci. Technol. 4 (2014) 2302–2311.
[19] C.M. Lew, N. Rajabbeigi, M. Tsapatsis, Microporous Mesoporous Mater. 153 (2012) 55–58.
[20] J.P. Lorenti, E. Scolari, E.M. Albuquerque, M.A. Fraga, J.M.R. Gallo, Appl. Catal. A Gen. 581 (2019) 37–42.
[21] B. Murillo, A. Sánchez, V. Sebastián, C. Casado-Coterillo, O. de la Iglesia, M.P. López-Ram- de-Viu, C. Téllez, J. Coronas, J. Chem. Technol. Biotechnol. 89 (2014) 1344–1350.
[22] L. Li, C. Stroobants, K. Lin, P.A. Jacobs, B.F. Sels, P.P. Pescarmona, Green Chem. 13 (2011) 1175–1181.
[23] C. Tempelman, U. Jacobs, T. Hut, E. Pereira de Pina, M. van Munster, N. Cherkasov, V. Degirmenci, Appl. Catal. A Gen. 588 (2019) 117267.
[24] I. Delidovich, R. Palkovits, ChemSusChem 9 (2016) 547–561.
[25] P.Y. Dapsens, C. Mondelli, J. Pérez-Ramírez, Chem. Soc. Rev. 44 (2015) 7025–7043.
[26] C.M. Osmundsen, M.S. Holm, S. Dahl, E. Taarning, P. Roy, Soc. A Math. Phy. 468 (2012) 2000–2016.
[27] E.T.C. Vogt, B.M. Weckhuysen, Chem. Soc. Rev. 44 (2015) 7342–7370.
[28] R. Netrabukkana, K. Lourvanij, G.L. Rorrer, Ind. Eng. Chem. Res. 35 (1996) 458–464.
[29] I. Graça, D. Iruretagoyena, D. Chadwick, Appl. Catal. B 206 (2017) 434–443.
[30] I. Graça, M.C. Bacariza, A. Fernandes, D. Chadwick, Appl. Catal. B 224 (2018) 660–670.
[31] I. Graça, M.C. Bacariza, D. Chadwick, Microporous Mesoporous Mater. 255 (2018) 130–139.
[32] C. Moreau, R. Durand, A. Roux, D. Tichit, Appl. Catal. A Gen. 193 (2000) 257–264.
[33] L. Hu, Z. Wu, J. Xu, Y. Sun, L. Lin, S. Liu, Chem. Eng. J. 244 (2014) 137–144.
[34] N.A.S. Ramli, N.A.S. Amin, Chem. Eng. J. 283 (2016) 150–159.
[35] N.A.S. Ramli, N.A.S. Amin, Appl. Catal. B 163 (2015) 487–498.
[36] Z. Wei, C. Dang-guo, Z. Huanhuan, C. Fengqiu, Z. Xiaoli, React. Kinet. Mech. Catal. 100 (2010) 377–384.
[37] K. Lourvanij, G.L. Rorrer, Appl. Catal. A Gen. 109 (1994) 147–165.
[38] P.Y. Dapsens, C. Mondelli, B.T. Kusema, R. Verel, J. Pérez-Ramírez, Green Chem. 16 (2014) 1176–1186.
[39] X. Yang, L. Wu, Z. Wang, J. Bian, T. Lu, L. Zhou, C. Chen, J. Xu, Catal. Sci. Technol. 6 (2016) 1757–1763.
[40] P.Y. Dapsens, B.T. Kusema, C. Mondelli, J. Pérez-Ramírez, J. Mol. Catal. A Chem. 388-389 (2014) 141–147.
[41] P.Y. Dapsens, M.J. Menart, C. Mondelli, J. Pérez-Ramírez, Green Chem. 16 (2014) 589–593.
[42] C.W. Kim, H.-C. Kang, N.H. Heo, K. Seff, J. Phys. Chem. C 118 (2014) 11014–11025.
[43] G.T. Kerr, J. Phys. Chem. 71 (1967) 4155–4156.
[44] R.M. Ravenelle, F. Schüßler, A. D'Amico, N. Danilina, J.A. van Bokhoven, J.A. Lercher, C.W. Jones, C. Sievers, J. Phys. Chem. C 114 (2010) 19582–19595.
[45] M. Wojdyr, J. Appl. Crystallogr. 43 (2010) 1126–1128.
[46] R.K. Harris, E.D. Becker, S.M. Cabral de Menezes, R. Goodfellow, P. Granger, Solid State Nucl. Magn. Reson. 22 (2002) 458–483.
[47] P.B.J. Thompson, B.N. Nguyen, R. Nicholls, R.A. Bourne, J.B. Brazier, K.R.J. Lovelock, S.D. Brown, D. Wermeille, O. Bikondoa, C.A. Lucas, T.P.A. Hase, M.A. Newton, J. Synchrotron Radiat. 22 (2015) 1426–1439.
[48] E.A. Pidko, V. Degirmenci, R.A. Van Santen, E.J.M. Hensen, Angew. Chem. Int. Ed. 49 (2010) 2530–2534.
[49] C. Huang, A. Li, Z.-S. Chao, RSC Adv. 7 (2017) 48275–48285.
[50] L. Hillen, V. Degirmenci, Rev. Adv. Sci. Eng. 4 (2015) 147–162.
[51] J. Sanz, V. Fornés, A. Corma, J. Chem. Soc. Farad. Trans. 1 84 (1988) 3113–3119.
[52] B. Tang, W. Dai, G. Wu, N. Guan, L. Li, M. Hunger, ACS Catal. 4 (2014) 2801–2810.
[53] M.P. Pachamuthu, K. Shanthi, R. Luque, A. Ramanathan, Green Chem. 15 (2013) 2158–2166.
[54] M. Xin, E. Xing, X. Gao, Y. Wang, Y. Ouyang, G. Xu, Y. Luo, X. Shu, Ind. Eng. Chem. Res. 58 (2019) 6970–6981.
[55] Y. Yu, G. Xiong, C. Li, F.-S. Xiao, J. Catal. 194 (2000) 487–490.
[56] Y. Xin, P. Qi, X. Duan, H. Lin, Y. Yuan, Catal. Lett. 143 (2013) 798–806.
[57] J. Dijkmans, D. Gabriëls, M. Dusselier, F. de Clippel, P. Vanelderen, K. Houthoofd, A. Malfliet, Y. Pontikes, B.F. Sels, Green Chem. 15 (2013) 2777–2785.
[58] S. Samanta, N.K. Mal, A. Manna, A. Bhaumik, Appl. Catal. A Gen. 273 (2004) 157–161.
[59] J.N. Chheda, Y. Román-Leshkov, J.A. Dumesic, Green Chem. 9 (2007) 342–350.
[60] L. Yang, G. Tsilomelekis, S. Caratzoulas, D.G. Vlachos, ChemSusChem 8 (2015) 1334–1341.
[61] S.K.R. Patil, J. Heltzel, C.R.F. Lund, Energ. Fuel. 26 (2012) 5281–5293.
[62] Y. Román-Leshkov, J.N. Chheda, J.A. Dumesic, Science 312 (2006) 1933.
[63] A.S. Amarasekara, L.D. Williams, C.C. Ebede, Carbohydr. Res. 343 (2008) 3021–3024.
[64] A. Ranoux, K. Djanashvili, I.W.C.E. Arends, U. Hanefeld, ACS Catal. 3 (2013) 760–763.